JOURNAL OF EXPERIMENTAL AND THEORETICAL PHYSICS, 2024, Vol. 165, No. 5, pp. 693–706

ORDER, DISORDER, AND PHASE TRANSITION IN CONDENSED MEDIA

CONTROLLING THE TEMPERATURE OF THE SPIN–REORIENTATION TRANSITION IN $HOFE_{1-X}MN_XO_3$ ORTHOFERRITE SINGLE CRYSTALS

© 2024 *K. A. Shaykhutdinov [a]*, S. A. Skorobogatov [a], Yu. V. Knyazev [a], T. N. Kamkova [a,b], A. D. Vasil'ev [a,b], S. V. Semenov [a,b], M. S. Pavlovskii [a,b], A. A. Krasikov [a]*

[a] *Kirensky Institute of Physics, Federal Research Center KSC SB RAS, Krasnoyarsk, 660036 Russia*
[b] *Siberian Federal University, Krasnoyarsk 660041, Russia*

Received November 08, 2023
Revised December 28, 2023
Accepted December 28, 2023

Abstract. $HoFe_{1-x}Mn_xO_3$ $(0 < x < 1)$ single crystals have been grown by the optical floating zone technique. A structural transition from the orthorhombic to hexagonal modification has been established in the crystals in the concentration range of 0.7–0.8, which has been confirmed by the X–ray diffraction data. For a series of the rhombic crystals, the room-temperature Mössbauer study and magnetic measurements in the temperature range of 4.2–1000 K have been carried out. It has been observed that, with an increase in the manganese content in the samples, the temperature of the spin-reorientation transition increases significantly: from 60 K in the $HoFeO_3$ compound to room temperature in $HoFe_{0.6}Mn_{0.4}O_3$. The magnetic measurements have shown that, upon substitution of manganese for iron, the magnetic orientational type transition changes from a second-order transition ($A_xF_yG_z \rightarrow C_xG_yF_z$) to first-order one ($A_xF_yG_z \rightarrow G_xC_yA_z$) with a weak ferromagnetic moment only in the **b** direction (for Pnma notation). The growth of the spin-reorientation transition temperature has been attributed to the change in the value of the indirect exchange in the iron subsystem under the action of manganese, which has been found when studying the Mössbauer effect in the $HoFe_{1-x}Mn_xO_3$ $(x < 0.4)$ compound.

DOI: 10.31857/S004445102405e080

1. INTRODUCTION

Oxide materials containing transition and rare-earth ions exhibit many intriguing effects caused by the complex interplay of two magnetic subsystems. Orthoferrites with the general formula $R\mathrm{FeO_3}$ [1–5] that can be distinguished into a separate class of such materials have been explored for more than half a century. The $R\mathrm{FeO_3}$ crystal structure is described by the sp. gr. Pnma (#62). Although the magnetic properties of these compounds have been thoroughly investigated, interest in them has grown again due to the recent discovery of a number of attracting phenomena: multiferroism below the temperature of ordering of the rare-earth subsystem [5, 6], laser-induced ultrafast magnetization switching in domain walls [7–9], formation of a soliton lattice in the $TbFeO_3$ compound [10], and existence of quasi-one-dimensional Yb^{3+} spin chains in the $YbFeO_3$ compound [5, 11].

Rare-earth orthoferrites represent a family with the extraordinary magnetic phenomena. The unique magnetic properties of these materials result from the complex interplay of the moments of 3d and 4f electrons. It is known well [1] that the $R\mathrm{FeO_3}$ compounds are characterized by unusually high Néel temperatures ($T_\mathrm{N}\sim$ 600–700 K), below which the Fe moments are ordered antiferromagnetically with a weak sublattice canting, which induces weak ferromagnetism. As the temperature decreases, the role of the Fe–R interaction increases; as a result, orientational spin transitions T_SR occur at lower temperatures, which depend strongly on the rare-earth ion: $T_\mathrm{SR}\approx$ 50–60 K for $HoFeO_3$ [12,13], $T_\mathrm{SR}\approx$ 80–90 K for $TmFeO_3$ [12,14], and $T_\mathrm{SR}\approx$ 3–10 K when Tb is used as a rare-earth element [10, 15]. Of special interest is the $SmFeO_3$ compound [16], in which the orientational transition is observed at $T_\mathrm{SR}\approx$ 450–480 K. The subsystem of rare-earth ions with a relatively weak R - R interaction at high temperatures is paramagnetic or weakly polarized by the molecular field of ordered Fe ions. The rare-earth magnetic sublattice becomes ordered below $T_\mathrm{SR}<$ 10 K (the temperature of ordering of the rare-earth subsystem). The observed magnetic properties of the system result from the multiplicity of different exchanges. In addition to the Fe–Fe, Fe–R,

* E-mail: smp@iph.krasn.ru

and R–R Heisenberg exchange couplings, an important role in determining the magnetic properties is played by the Dzyaloshinskii–Moriya interaction [17,18], which induces a weak ferromagnetic moment.

A way of controlling the temperature of the spin-reorientation transition is isovalent substitution in the $R\mathrm{Fe}_{1-x}M_x\mathrm{O}_3$ (M = Cr, Mn, Co, Ni) iron subsystem. In this case, it becomes possible to smoothly change the magnetic properties in such systems and set the desired temperature T_{SR}, for example, at the ultrafast magnetization switching in domain walls [7–9]. For example, in [19], the reversible spin-reorientation transition was observed in the $\mathrm{TbFe}_{0.75}\mathrm{Mn}_{0.25}\mathrm{O}_3$ single crystal at $T_{\mathrm{SR}} = 250$ K, whereas in the pure TbFeO_3 single crystal, the transition occurs at temperatures of 3 and 8 K. In [20], a $\mathrm{SmFe}_{0.75}\mathrm{Mn}_{0.25}\mathrm{O}_3$ single crystal was successfully grown; it was shown that, when a part of iron is replaced by manganese, the temperature T_{SR} decreases noticeably. In [21], the authors managed to grow a series of $\mathrm{PrFe}_{1-x}\mathrm{Mn}_x\mathrm{O}_3$ ($0 < x < 0.3$) single crystals and demonstrated that, at a manganese content of 30%, the spin-reorientation transition shifts to room temperature. In [22], the synthesis of a series of $\mathrm{GdFe}_{1-x}\mathrm{Mn}_x\mathrm{O}_3$ ($0 < x < 0.3$) single crystals was reported. In recent study [23], the authors reported on the successful growth of the $\mathrm{Nd}_{0.8}\mathrm{Pr}_{0.2}\mathrm{FeO}_3$ single crystal and the observed drop in the T_{SR} value upon such substitution.

It should be noted that the majority of studies have been carried out on polycrystalline samples. Meanwhile, in terms of the potential of the discussed orthoferrites for microelectronic applications, it is desirable to explore their single-crystal samples. We can distinguish studies [24–26] aimed at the examination of dysprosium, terbium, and yttrium orthoferrites with partial substitution of manganese for iron; in these materials, a change in the temperature T_{SR} was also observed. In addition, in some works [27–29], substitution of other transition elements (chromium, nickel, and cobalt) into the iron subsystem was performed and a change in the T_{SR}value was reported.

Concerning the $\mathrm{HoFe}_{1-x}\mathrm{Mn}_x\mathrm{O}_3$ compound, in [30, 31] the polycrystalline $\mathrm{HoFe}_{1-x}\mathrm{Mn}_x\mathrm{O}_3$ ($0 < x < 0.5$) samples were synthesized and their magnetic and structural features were reported. It was shown that, at a concentration of $x = 0.4$, the temperature T_{SR} for this compound reached room temperature. However, against the background of holmium paramagnetism, the spin-reorientation transition turns into just a minor anomaly in the magnetization curve. Therefore, to study the evolution of the magnetic properties in more detail, it is necessary to perform measurements on single-crystal samples.

The aim of this study was to grow and investigate single-crystal $\mathrm{HoFe}_{1-x}\mathrm{Mn}_x\mathrm{O}_3$ samples with a manganese content of up to its maximum value at which this solid solution remains stable in the orthorhombic phase. For potential use of orthoferrites in spin switching devices and magnetic storage cells operating at room temperature, single-crystal samples are also needed.

Thus, we can summarize that the isovalent substitution in orthoferrites has been investigated in quite a lot of studies, with the main focus on the variation in the temperature of orientational transitions in these materials. In the studies on the single-crystal samples, the minor substitutions (as a rule, with $x < 0.3$) in the iron subsystem was used. The aim of this study was to grow and investigate single-crystal $\mathrm{HoFe}_{1-x}\mathrm{Mn}_x\mathrm{O}_3$ samples with a manganese content of up to its maximum value at which this solid solution remains stable in the orthorhombic phase. In addition, we attempted to grow $R\mathrm{Fe}_{1-x}M_x\mathrm{O}_3$ (M = Cr, Mn, Co, Ni) single crystals with $x > 0.05$, since, according to the literature data [32], the samples of this compound with a concentration range of $x < 0.05$ have already been synthesized.

Here, it should be mentioned that Mössbauer spectroscopy yields valuable information on the spin-reorientation transition [35–38], since it provides direct observations of an angle between the hyperfine magnetic field on nuclei and the direction of the electric field gradient induced by the crystal field in a substance [39].

2. EXPERIMENTAL DETAILS

At the first stage, to obtain the $\mathrm{HoFe}_{1-x}\mathrm{Mn}_x\mathrm{O}_3$ ($x = 0, 0.05, 0.1, 0.2, 0.3, 0.4, 0.5, 0.6, 0.7$, and 0.8) samples, the initial $\mathrm{Ho_2O_3}$, $\mathrm{Fe_2O_3}$, and $\mathrm{MnO_2}$ powders (99.9%, Alfa Aesar) were mixed in required proportions and subjected to annealing at a temperature of 925 °C for 18 h. The annealed powders were poured into a rubber mold and pressed in a hydrostatic press at a pressure of $\sim$ 100 MPa. The resulting cylindrical samples were then annealed in a vertical furnace at 1400 °C for 16 h. After that, the synthesized polycrystalline $\mathrm{HoFe}_{1-x}\mathrm{Mn}_x\mathrm{O}_3$ samples were placed in an FZ–T–4000–H–VIII–VPO–PC optical floating zone furnace (Crystal Systems Corp.) to grow single crystals. The crystal growth occurred in air at a normal pressure and a relative rod rotation speed of 30 rpm. The growth rates varied from 3 to 1 mm/h,

depending on the ratio between iron and manganese in the $HoFe_{1-x}Mn_xO_3$ composition. It should be noted that we attempted to grow the $HoFe_{1-x}Co_xO_3$, $HoFe_{1-x}Cr_xO_3$, and $HoFe_{1-x}Ni_xO_3$ single crystals with $x = 0.05$; however, substitution of even 5% of chromium or nickel for iron led to incongruent melting and did not allow us to obtain high-quality single crystals. The change in pressure (up to 10 atm) and a gaseous medium (O_2, Ar–O_2, or Ar–H_2) did not improve the growth conditions in this case. It also seemed that the $HoFe_{0.95}Co_{0.05}O_3$ single crystal was successfully grown, but the measured temperature dependences of the magnetization were found to be the same as for the $HoFeO_3$ crystal, which showed that cobalt was not substituted for iron during the growth.

To solve the crystal structure and determine the phase purity of the $HoFe_{1-x}Mn_xO_3$ compound, a Bruker SMART APEX II single-crystal X–ray diffractometer was used. The measurements were performed at room temperature. The crystallographic orientations of all the single crystals were determined on a Photonic Science Laue Crystal Orientation System by the back reflection method. Mössbauer spectra for the investigated samples were obtained on an MS–1104Em spectrometer in the transmission geometry with a $^{57}Co(Rh)$ radioactive source at a temperature of 300 K. Temperature and field dependences of the magnetization of the grown single crystals were obtained on a Quantum Design Physical Property Measurement System (PPMS–6000) in the temperature range of 4.2–350 K. The high-temperature (350–1000 K) magnetization measurements were performed on a Lake Shore Cryotronics VSM–8604 vibrating sample magnetometer. After temperature cycling up to 1000 K, the repeatability of the characteristic (Néel and spin-reorientation) temperatures and the magnetization values were checked. All the measurements were found to be fully repeatable.

3. RESULTS AND ANALYSIS

3.1. Structure characterization

To check the quality of all the grown $HoFe_{1-x}Mn_xO_3$ single crystals and their orientations along the three crystallographic axes, the Laue method was used. As an example, Fig. 1 presents Lauegrams of the sample with $x = 0.3$ corresponds to the reflection planes with indices (100), (010), (001) (Figs. 1 (a, b, c)) and the sample with $x = 0.8$ (Fig. 1d) for the reflection plane (0001). The observed sharp symmetric

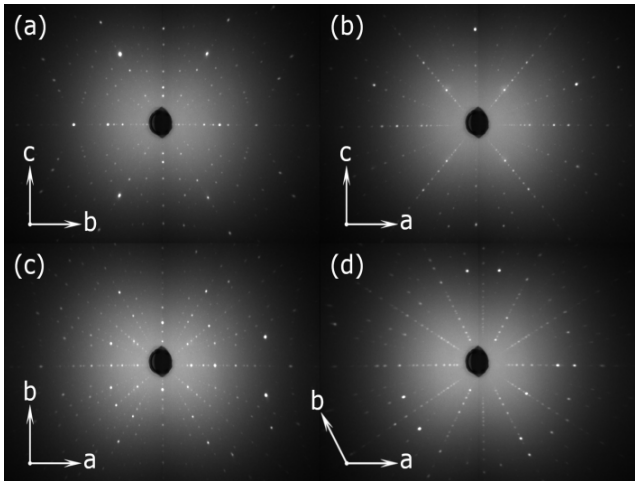

Fig 1. Lauegrams of (a, b, c) the $HoFe_{0.7}Mn_{0.3}O_3$ sample from reflection planes (100), (010), (001) and (d) the $HoFe_{0.2}Mn_{0.8}O_3$ sample from reflection plane (0001). The direction of the crystallographic axes relative to the reflection plane is shown in each figure.

peaks and the absence of twinning are indicative of the high quality of the synthesized crystals. In addition, the reflections for the sample with $x = 0.3$ correspond to the sp. gr. Pnma (#62), while the Lauegram of the sample with $x = 0.8$ corresponds to the sp. gr. P63cm (#185). Thus, upon substitution of manganese for iron in the $HoFe_{1-x}Mn_xO_3$ ($0.7 < x < 0.8$) sample, the interface between the orthorhombic and hexagonal modifications in the $HoFe_{1-x}Mn_xO_3$ solid solution is observed. We note that the single crystal with $x = 1$ (pure $HoMnO_3$) in the orthorhombic modification can be obtained by the solution–melt method [40], which makes it possible to significantly lower the melt temperature, whereas the optical floating zone technique yields only the hexagonal $HoMnO_3$ modification [41]. Based on the obtained data on the interface in $HoFe_{1-x}Mn_xO_3$, below we present the results of investigations of the orthorhombic $HoFe_{1-x}Mn_xO_3 (x < 0.7)$ single crystals synthesized by zone melting under the same conditions.

From the results of single-crystal X-ray diffraction analysis, it was also found that all $HoFe_{1-x}Mn_xO_3$ single crystals with ($x < 0.7$) are rhombic with space group Pnma, this notation is standard. In some works by other authors, a notation with a Pbnm spatial symmetry group was used, the transition from one notation to another can be described as follows: $a, b, c(Pnma) \rightarrow b, c, a(Pbnm)$. Their lattice parameters are given in Table 1 and presented in Fig. 2.

It can be seen from Table 1 and Fig. 2 that, under the isovalent substitution of manganese for

Table 1. Lattice parameters, unit cell volumes in the $HoFe_{1-x}Mn_xO_3$ compound.

x	a	b	c	V
0	5.6029(5)	7.6151(7)	5.2921(5)	225.80(5)
0.05	5.6133(3)	7.6102(5)	5.2885(3)	225.92(2)
0.1	5.6201(5)	7.5990(4)	5.2840(3)	225.66(2)
0.2	5.6425(3)	7.5801(4)	5.2864(3)	226.10(2)
0.3	5.6608(3)	7.5551(3)	5.2826(2)	225.93(2)
0.4	5.6911(4)	7.5411(5)	5.2840(4)	226.77(3)
0.5	5.7065(3)	7.5080(4)	5.2779(3)	226.73(3)
0.6	5.7085(3)	7.5029(3)	5.2768(2)	226.01(2)
0.7	5.7385(3)	7.4688(4)	5.2728(3)	225.99(3)

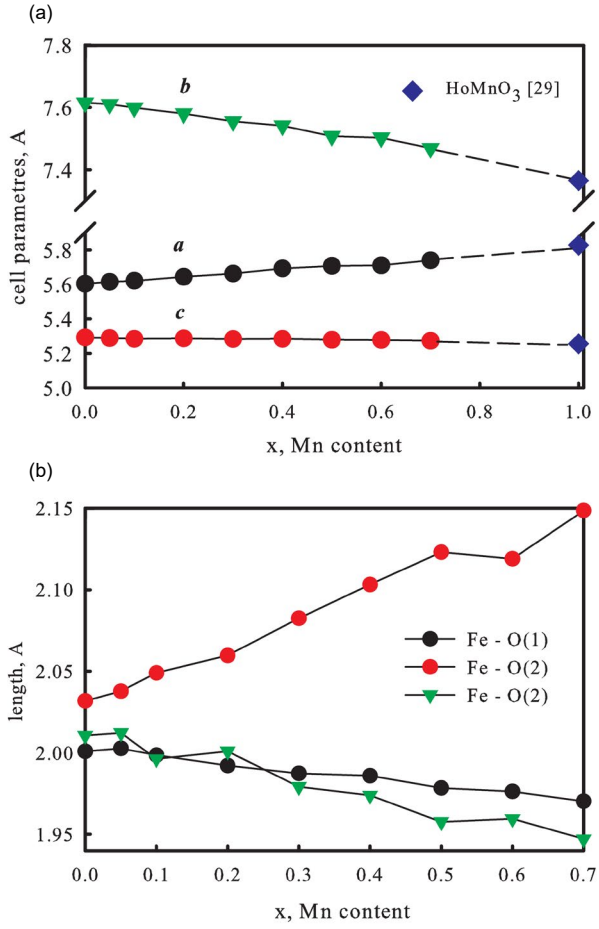

Fig. 2. (a) $HoFe_{1-x}Mn_xO_3$ lattice parameters vs manganese content. Blue diamonds show the lattice parameters of the $HoMnO_3$ crystal from [40]. (b) Manganese content dependence of Fe–O(1) and Fe–O(2) bond lengths in the iron–oxygen octahedron.

iron in the $HoFe_{1-x}Mn_xO_3$ ($x < 0.7$) compound, the lattice parameters change linearly over the entire concentration range. In this case, parameter **a** increases linearly, parameter **b** decreases, and parameter **c** decreases insignificantly; the unit cell volume remains almost unchanged. Figure 2 presents the concentration dependence of Fe–O(1) and Fe–O(2) bond lengths in the iron–oxygen octahedron. It can be seen that, as the x value increases, the octahedron shrinks along the **b** direction and the greatest changes occur in the octahedron plane close to the **ac** plane, where the Fe–O(2) bond significantly elongates. Using the single–crystal X–ray diffraction data, we can determine the direction of the main component of the electric field gradient (EFG) tensor V_{zz}, which conventionally determines the principal axis direction in the octahedron. The V_{zz} can be determined from the X–ray diffraction data using the known bond lengths and angles in the octahedral environment of iron in the nearest neighbor approximation [39] as

$$V_{zz} = \sum 2e\frac{3cos^2(\theta) - 1}{r^3} \qquad (1)$$

Where V_{zz} is the EFG in the direction of the principal axis of the oxygen octahedron, θ is the angle between this axis and the direction to the neighboring oxygen ion, e is the elementary charge, and r is the metal–oxygen distance. In the calculation, all possible directions of the EFG axis in the local environment of the cation are checked, after which the main component of the EFG tensor is selected according to the condition $|V_{zz}| \geq |V_{yy}| \geq |V_{xx}|$.

The results of the calculation in all possible directions for all the samples are given in Table 2 and presented in Fig. 3. Thus, we determine the direction of the main component of the EFG tensor relative to the crystallographic axes (shown in blue in the inset to Fig.3). The chemical bond length in this direction exceeds the lengths in the two other directions, so the oxygen octahedron is elongated.

Table 2. Metal–oxygen distances at different Mn contents.

x	$M-O1(4c)$	$M-O2(8d)$	$M-O2(8d)$
0	2.001	2.011	2.032
0.05	2.003	2.012	2.038
0.1	1.998	1.996	2.049
0.2	1.992	2.001	2.060
0.3	1.987	1.979	2.082
0.4	1.986	1.974	2.103

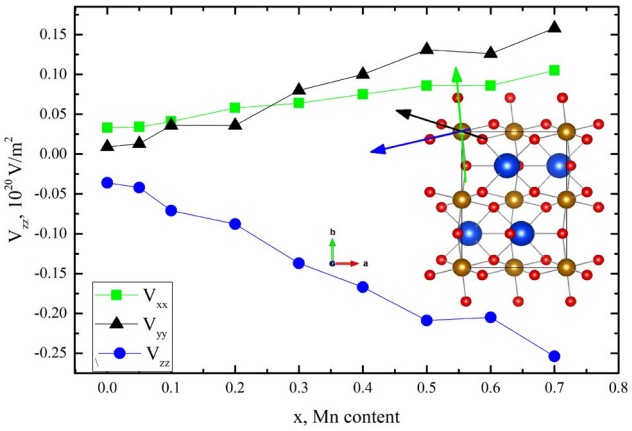

Fig 3. EFG tensor components vs Mn content in the $HoFe_{1-x}Mn_xO_3$ compound. The inset shows the directions of all the components of the EFG vector relative to the crystallographic axes.

3.2. Mössbauer Spectroscopy Study

Samples for the Mössbauer spectroscopy study were prepared by grinding the $HoFe_{1-x}Mn_xO_3$ ($0 < x < 0.4$) single crystals to a powder. The powder sample with a weight of 5–10 g/cm^2 according to the iron content was pressed in aluminum foil 20 mm in diameter. The processing occurred in two stages. At the first stage, possible nonequivalent positions of iron in the samples were determined by calculating the hyperfine field probability distributions. Basing on the results obtained, a preliminary model spectrum was formed. At the next stage, the model spectrum was fitted to the experimental spectrum by varying the entire set of hyperfine parameters using the least squares method in the linear approximation.

The spectra obtained are shown in Fig. 4. These are fully resolved Zeeman sextets, the parameters of which are listed in Table 3. The chemical shift δ for all the samples relative to α–Fe indicates the 3+ charge state of high-spin iron cations in the octahedral environment, which is consistent with the crystal structure of orthoferrites and the previous Mössbauer data [42, 43]. Under the increasing substitution of Mn^{3+} cations up to $x = 0.20$, an additional iron site appears, which corresponds to a sextet with a strong hyperfine field. The fraction of this sextet increases stepwise and remains almost invariable in the concentration range of $x = 0.20$–0.40, which may indicate that manganese cations occupy certain positions in the lattice at these concentrations. This is indirectly confirmed by two characteristic segments in the concentration dependence of the average hyperfine field on iron nuclei, which remains monotonic (Fig. 5).

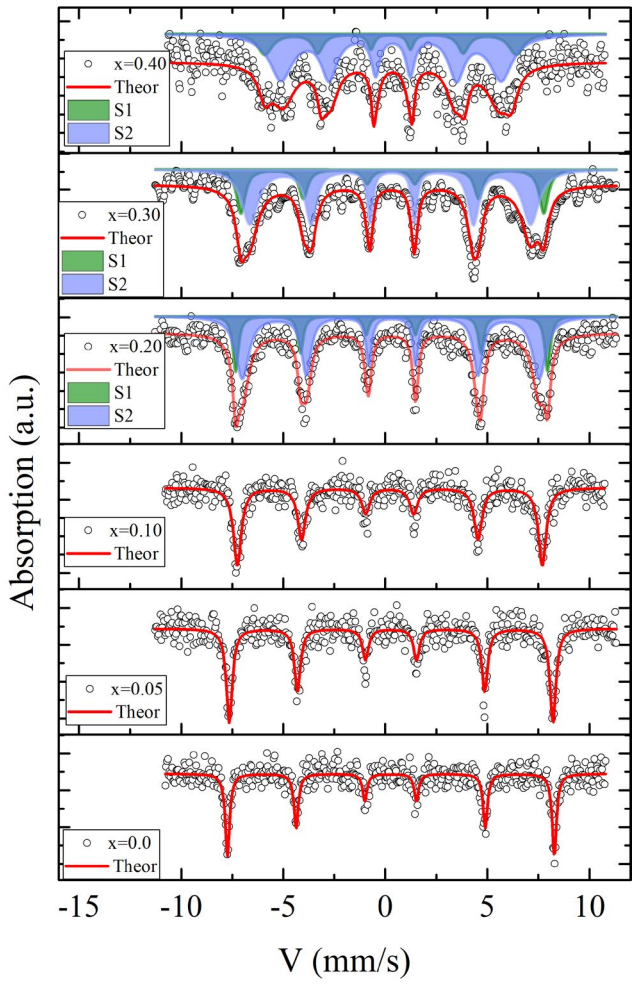

Fig 4. Mössbauer spectra of the $HoFe_{1-x}Mn_xO_3$ ($x = 0, 0.05, 0.10, 0.20, 0.30,$ and 0.40) samples. The solid line shows the processing results. The shaded areas show partial components in the spectra.

Let us focus on the dependence of quadrupole shift $\triangle$ of the main sextet on the manganese content in the $HoFe_{1-x}Mn_xO_3$ single crystal (Fig. 6). We can see a monotonic decrease in the quadrupole shift with the increasing Mn content in the samples. Simultaneously, we note the change of the $\triangle$ sign at a Mn content of $x = 0.20$ for the sextet with a larger area. This can be explained by the effect of the single–ion anisotropy of manganese cations, which essentially contributes to the formation of the EFG tensor. As for the behavior of the second sextet quadrupole shift, its sign remains invariable over the entire concentration range and its value changes insignificantly with an increase in the degree of substitution.

The quadrupole shift of the Mössbauer spectrum originates from (i) local distortions of the crystal lattice and (ii) the mutual direction of vectors V_{zz} and H_{hf}.

Table 3. Mössbauer parameters at 300 K. δ – is the isomer chemical shift relative to α–Fe, H_{hf} – is the hyperfine field on iron nuclei, $\triangle$ – is the quadrupole splitting, W – is the Mössbauer line full width at half maximum, dH – is the Mössbauer line broadening due to the inhomogeneity of the magnetic environment, and A – is the relative site occupancy.

	δ, ±0.005 mm/s	H_{hf}, ±5 kOe	$\triangle$, ±0.02 mm/s	W, ±0.03 mm/s	dH, ±0.03 mm/s	A, ±0.03 $arb.u.$
$HoFeO_3$						
$S1$	0.387	498	0.02	0.26	0	1.0
$x = 0.05$						
$S1$	0.374	492	0.00	0.20	0.20	1.0
$x = 0.10$						
$S1$	0.382	465	−0.00	0.46	0	1.0
$x = 0.20$						
$S1$	0.402	452	−0.14	0.25	0.54	0.73
$S2$	0.388	475	0.08	0.33	0	0.27
$x = 0.30$						
$S1$	0.368	409	−0.19	0.21	0.73	0.70
$S2$	0.388	441	0.12	0.51	0	0.30
$x = 0.40$						
$S1$	0.427	335	−0.20	0.37	0.98	0.75
$S2$	0.361	383	0.08	0.31	0.58	0.25

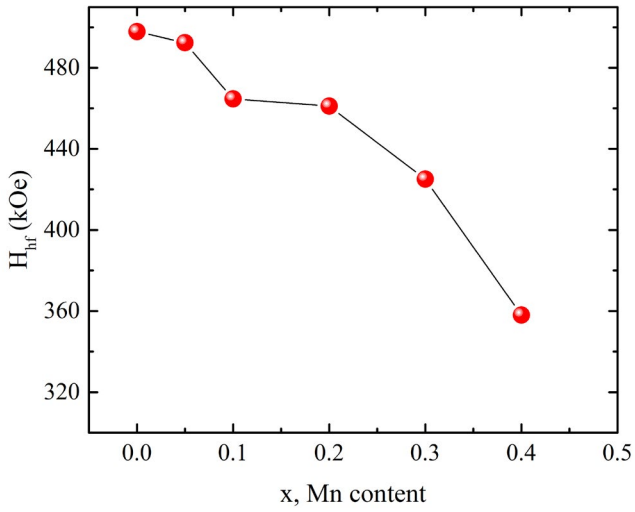

Fig 5. Concentration dependence of the average hyperfine field on iron nuclei in the $HoFe_{1-x}Mn_xO_3$ compound.

The former determine the lattice contribution to the quadrupole splitting in the paramagnetic state, which

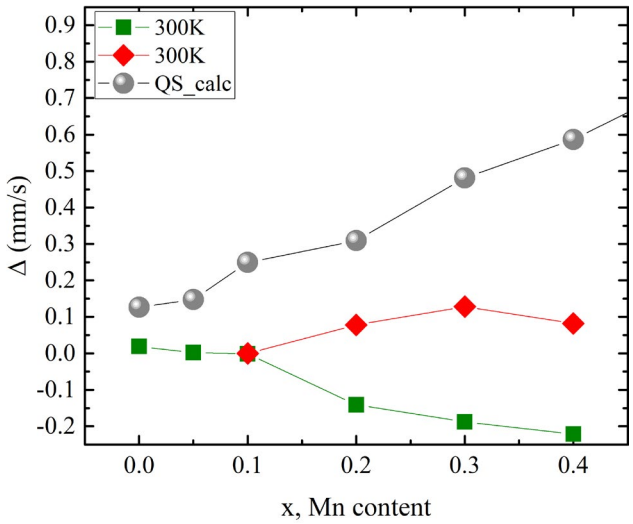

Fig 6. Concentration dependence of quadrupole shift $\triangle$ in the $HoFe_{1-x}Mn_xO_3$ ($0 < x < 0.4$) samples. Spheres show the QS values calculated from the X–ray diffraction data.

can be found, with allowance for the Sternheimer antiscreening effect [44, 45] as

$$QS = (1 - \gamma_\infty)\frac{1}{2}eQV_{zz}(1 + \frac{\eta^2}{3})^{1/2} \qquad (2)$$

Here, $\gamma_\infty = -9.44$ is the Sternheimer antiscreening factor for a spherically symmetric Fe^{3+} cation [46] and $\eta = (V_{xx} - V_{yy})/V_{zz}$ is the a symmetry parameter, which describes the deviation from the axial symmetry.

In our case, the change in local distortions upon substitution is taken into account in the V_{zz} value calculated from the X–ray diffraction data. It should be noted that the approach used ignores the covalent contribution of chemical bond electrons to the quadrupole splitting. In our case, however, this contribution for the Fe^{3+} cation can be neglected. The calculated data are shown by spheres in Fig. 6. For the $HoFeO_3$ sample, the calculated $\triangle$ value is 0.13 mm/s, while the experimental value in the paramagnetic state is 0.30 mm/s, as reported [42]. We attribute the obtained discrepancy with the experiment to the valence contribution.

3.3. Magnetic Measurements

To elucidate the effect of manganese substitution on the magnetic properties of the $HoFe_{1-x}Mn_xO_3$ compounds, the temperature and field dependences of the magnetization M were measured. Figure 7 shows the $M(T)$ dependences measured in the magnetic field $H||\mathbf{b}$. It can be seen that, as the manganese content

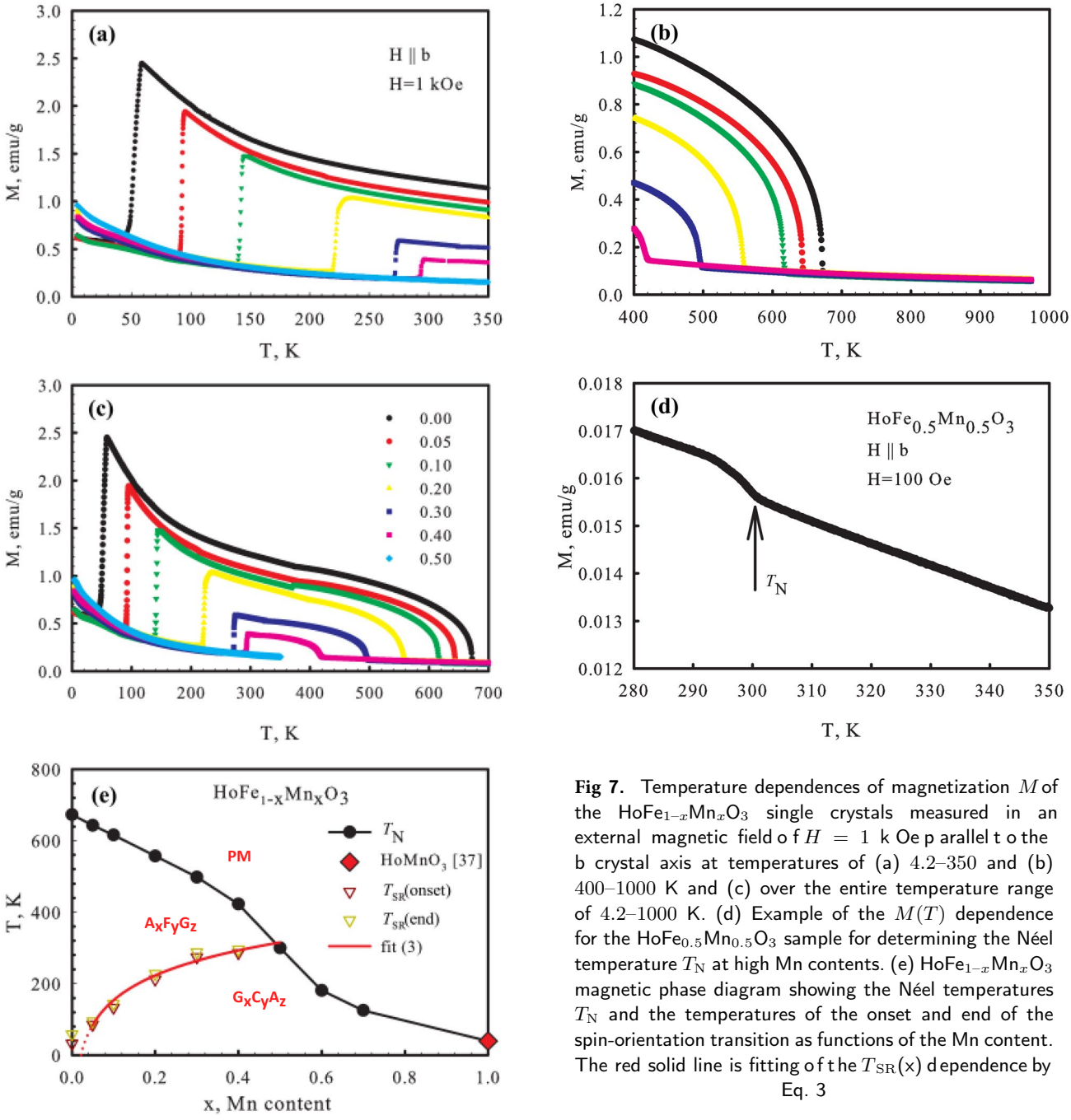

Fig 7. Temperature dependences of magnetization M of the $HoFe_{1-x}Mn_xO_3$ single crystals measured in an external magnetic field of $H = 1$ kOe parallel to the b crystal axis at temperatures of (a) 4.2–350 and (b) 400–1000 K and (c) over the entire temperature range of 4.2–1000 K. (d) Example of the $M(T)$ dependence for the $HoFe_{0.5}Mn_{0.5}O_3$ sample for determining the Néel temperature T_N at high Mn contents. (e) $HoFe_{1-x}Mn_xO_3$ magnetic phase diagram showing the Néel temperatures T_N and the temperatures of the onset and end of the spin-orientation transition as functions of the Mn content. The red solid line is fitting of the $T_{SR}(x)$ dependence by Eq. 3

increases, the temperature T_{SR} shifts monotonically to the high-temperature region. For the unsubstituted $HoFeO_3$ sample, we have $T_{SR} \approx 58$ K, while for the sample with $x = 0.4$, $T_{SR} = 294$ K; i.e., the T_{SR} values lie in the room-temperature region. The value of magnetization (M), which is determined by a weak ferromagnetic moment induced by canting of the iron antiferromagnetic sublattices, decreases gradually as the Mn content grows (Fig. 7a).

In addition, with an increase in the manganese content, the $HoFe_{1-x}Mn_xO_3$ Néel temperature decreases monotonically from $T_N = 672$ K for the $HoFeO_3$ compound to $T_N = 125$ K for the composition with $x = 0.7$ (Figs. 7 (b, c, e). An example of determining the Néel temperature of the samples with $x = 0.5, 0.6$, and 0.7 is presented in Fig. 7d; in Fig. 7d, at $x = 0.5$, the Néel temperature is

T_N= 300 K. The Néel temperatures of all the investigated $HoFe_{1-x}Mn_xO_3$ samples are shown in the phase diagram in Fig. 7e. The T_N value at $x = 1$ ($HoMnO_3$) was determined in [41]. It can be seen that, at concentrations of $x \approx 0.5$, the T_N(x) dependence has an inflection, which is possibly related to a change in the dominant antiferromagnetic interaction from Fe–O–Fe to Mn–O–Mn. In addition, $x = 0.4$–0.5 is the limiting concentration range, in which the spin-reorientation transition still occurs; with a further increase in the manganese content, T_N becomes lower than T_{SR}, which corresponds to the paramagnet–to–antiferromagnet phase transition without successive orientational transitions. Figure 7e shows also the dependence of the temperature T_{SR} on the Mn content x (red solid line) calculated using the

$$T_{SR}(x) = \frac{1}{k'} \lg(\frac{x}{x_c}) \qquad (3)$$

where k' is a positive constant related to the second–order anisotropy fields in the b–a, b–c, c–a planes. x_c characterizes a critical doping concentration from characterizes the critical concentration at which a transition to the state of a collinear antiferromagnet occurs (GxCyAz phase). In this study, the change in the second–order anisotropy constants responsible for the temperature of the spin–reorientation transition upon variation in the cobalt concentration in erbium, holmium, and dysprosium orthoferrites was investigated. In our opinion, this formalism [32] can be applied to describing the T_{SR}(x) change in the $HoFe_{1-x}Mn_xO_3$ compound. Previously, formula (3) was successfully used in [19–21].

It is known well that, during the spin–reorientation transition in the unsubstituted $HoFeO_3$ compound, the weak ferromagnetic moment rotates spontaneously by 90° from the **b** to **c** direction in the crystal ($Pnma$) from the $A_xF_yG_z$ to $C_xG_yF_z$ phase (Fig. 8); this is a second-order phase transition [3] (A, C, G are types of antiferromagnetic structures [3], F is ferromagnetic; for orthoferrites, the main type of the order parameter is the G type of antiferromagnetism with |G|»|F|, |A|,|C|). The temperature transition width for $HoFeO_3$ is ∼ 10 K, while no temperature hysteresis is observed. It should also be mentioned that according to previous works [33, 34] in pure $HoFeO_3$, the spin reorientation between the $A_xF_yG_z$ and $C_xG_yF_z$ states (in the Pnma notation) occurs in a more complex way in the form of three phase transitions: first, the main vector of antiferromagnetism G deviates from the **c** – to the **b** – axis in the **bc** plane, then, before reaching the **b** – axis, it abruptly reorients into the ab plane and it already

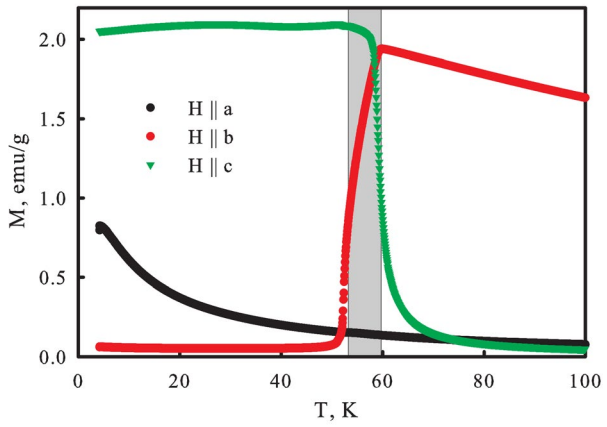

Fig 8. Temperature dependences of magnetization M of the $HoFeO_3$ compound measured in a field of $H = 100$ Oe along different crystallographic axes. The spin reorientation area is marked in gray.

rotates to the final state along the **b** – axis. Magnetic properties usually show only the first part (rotation in the **bc** plane) of this complex reorientation, and the rest was observed using measurements of magnetoelastic properties and magnetic resonance. In the substituted samples, we have a completely different picture.

First, as can be seen from the $M(T)$ dependences measured in the heating mode (Figs. 7 (a and c)), the width of the spin-reorientation transition in the substituted samples is about 4–5 K. Figure 9 shows the $M(T)$ dependences for the $HoFe_{0.7}Mn_{0.3}O_3$ sample measured in external magnetic fields of different values and configurations. According to Fig. 9a, the nature of the spin–reorientation transition in the substituted sample changed drastically: in the unsubstituted $HoFeO_3$ compound, the phase transition from the $A_xF_yG_z$ to $C_xG_yF_z$ phase occurs with a change in the weak ferromagnetic moment direction, while in the $HoFe_{0.7}Mn_{0.3}O_3$ compound, below the T_{SR} temperature, a compensated antiferromagnetic phase of the iron and manganese sublatticeis observed. In this case, the magnetization is only determined by the paramagnetic anisotropic contribution of holmium, which is reflected in the $M(T)$ dependences (Fig. 9a) measured along different crystallographic axes. In addition, it is noteworthy that, upon temperature cycling, the $M(T)$ dependences measured along the **b** direction in different magnetic fields (Fig. 9b) exhibit the hysteresis in the region of the transition (T_{SR}), the width of which amounts to ∼ 5 K regardless of the applied magnetic field (up to 5 kOe). In addition, it can be seen in Fig. 9b that the applied magnetic

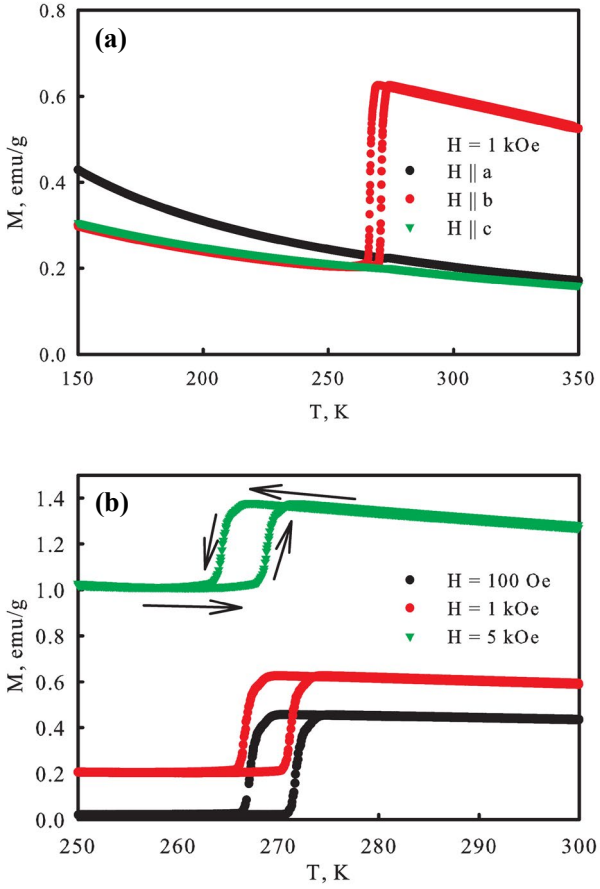

Fig. 9. (a) Temperature dependences of magnetization M of the $HoFe_{0.7}Mn_{0.3}O_3$ single crystal in the region of the spin–reorientation transition. (b) Temperature dependences of magnetization M measured in different applied magnetic fields H ||**b** i n t he c ooling a nd heating modes.

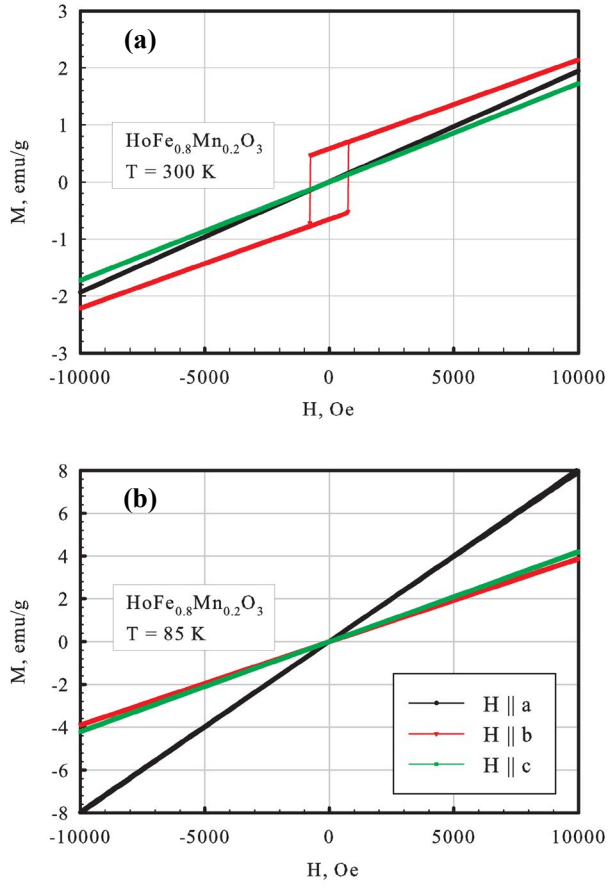

Fig 10. $M(H)$ dependences for the $HoFe_{0.8}Mn_{0.2}O_3$ single crystal at $T = 300$ and 85 K.

field affects weakly the T_{SR} temperature position; the onset of the transition shifts by 2 K toward lower temperatures in a field of $H = 5$ kOe and the transition is not blurred. Exactly the same $M(T)$ behavior is exhibited by all the substituted $HoFe_{1-x}Mn_xO_3$ samples, which only have different spin-reorientation transition temperature.

Figure 10 shows the field dependences of magnetization M of the $HoFe_{0.8}Mn_{0.2}O_3$ sample at temperatures above and below the temperature T_{SR} of the spin–reorientation transition along three crystallographic axes. It can be seen that the $M(H)$ ferromagnetic hysteresis is only observed along the **b** direction at $T > T_{SR}$, which corresponds to the $A_xF_yG_z$ magnetic phase (Fig. 10a). At temperatures of $T < T_{SR}$, all the $M(H)$ dependences are linear, which corresponds to the contribution of the collinear antiferromagnetic structure (the $G_xC_yA_z$ phase) without ferromagnetic component. The similar $M(H)$ behavior was observed by us for all the substituted samples.

Figure11 shows the $M(H)$ dependences measured at $T = 300$ K for all the $HoFe_{1-x}Mn_xO_3$ samples and the remanent magnetizations at $H = 0$ Oe and coercivities (switching fields) H_{sw}. The magnetization switching from the lower to upper branch occurs in a negligibly narrow field range, which means that the sample includes a single magnetic domain. In all the substituted samples at $T = 300$ K, the ferromagnetic magnetization component only exists along the **b** direction. Therefore, by changing the Mn content in the samples, one can smoothly change both the magnetization and coercivity value, which can be promising for use of this series of single crystals at room temperatures.

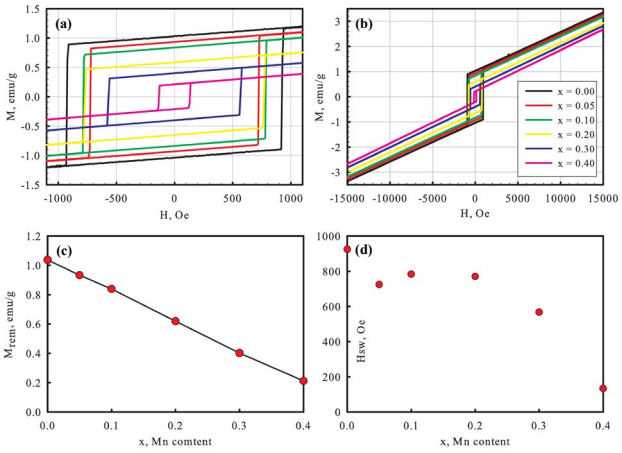

Fig. 11. (a, b) $M(H)$ dependences at $T = 300$ K for a series of the $HoFe_{1-x}Mn_xO_3$ samples. (c) Remanent magnetization at $H = 0$ and (d) switching field as functions of themanganese content.

4. DISCUSSION

It can be concluded from the analysis of the $M(T)$ dependences that, in manganese–substituted holmium orthoferrites, the spin–reorientation transition is a first-order phase transition [3], which determines the change in the magnetic state from the weak ferromagnetism region (the $A_xF_yG_z$ phase, the magnetic moment along the **b** crystal direction) to the fully compensated antiferromagnetic region (the $G_xC_yA_z$ phase). Such a change in the nature of the phase transition in the $HoFe_{1-x}Mn_xO_3$ compound was observed in [19], where this conclusion was made on the basis of the neutron powder diffraction data. The change in the magnetic transition configuration from $A_xF_yG_z \rightarrow C_xG_yF_z$ to $A_xF_yG_z \rightarrow G_xC_yA_z$ (in *Pnma* notation) was observed in the $TbFe_{1-x}Mn_xO_3$ compound in [18], where the type of magnetic ordering was also determined by neutron diffraction. In this work, we obtained the similar results by the thorough analysis of the temperature and field dependences of the magnetization. Meanwhile, some questions about the magnetic behavior of the investigated system remain open.

Until now, no attention has been paid to the origin and mechanism of the significant growth of the temperature of the magnetic spin-reorientation transition in the $HoFe_{1-x}Mn_xO_3$ system. The reasons for this phenomenon can be analyzed using the Mössbauer spectroscopy data. Since the replacement of a part of iron cations results in a change in the orbital momentum at the sites, the substitution will also change the spin–orbit coupling value. As a result, the magnetic moment direction will deviate from the quantization axis. This will lead to a change in the mutual orientation of the EFG (V_{zz}) vector and the hyperfine field vector (H_{hf}) on iron nuclei. In the case of the axial symmetry, this change is described by the dependence of the quadrupole shift [37, 47]

$$\triangle = \frac{e^2}{4} Q \cdot V_{zz} \frac{1}{2} (3cos^2(\theta) - 1) \qquad (4)$$

Here, Q is the quadrupole moment of a nucleus ($+0.21 \cdot 10^{-24}$ sm^{-2}), V_{zz} is the main component of the EFG tensor, θ is the angle between the EFG direction and the hyperfine field, and e is the elementary charge. It is reliably demonstrated by the magnetic measurement data that the temperature of the spin-reorientation transition in the $HoFe_{1-x}Mn_xO_3$ compound depends strongly on the degree of substitution. Since the crystal structure is preserved in this case, it can be assumed that the quadrupole moment of a nucleus does not change. This allows us to estimate the concentration dependence of the angle θ upon substitution using the Mössbauer spectroscopy data and Eq. 3.

Thus, taking into account the V_{zz} values obtained by X–ray diffraction, we can estimate the change in the mutual orientation of the vectors V_{zz} and H_{hf} under the substitution (Fig. 12). It can be clearly seen that the angle changes sharply at a Mn content of $x = 0.20$. Taking into account the known direction of the vector V_{zz} from Fig. 4, we can demonstrate that the magnetic moment direction (opposite to H_{hf}) becomes closer to the **ac** crystal plane at the incorporation of manganese (Fig. 8b). To explain the mechanism of changing the type of spin reorientation during manganese doping, one can also consider the contribution of Of Yahn-Teller Mn^{3+} ions into a single-ionic anisotropy. In rhombic manganites ($LaMnO_3$, $PrMnO_3$, $NdMnO_3$) [49, 50], it stabilizes the orientation of Mn^{3+} spins along the a axis in the weakly ferromagnetic $A_xF_yG_z$ structure, where the main order parameter, unlike orthoferrites, is A – type. The presence of such anisotropy of Mn^{3+} ions interchangeably bound to Fe^{3+} spins should contribute to the orientation of the latter along the a axis in the antiferromagnetic the structure of $G_xC_yA_z$ substituted compounds. This mechanism of stabilizationof the antiferromagnetic structure of G_xCyAz should also work for other compositions of Mn-substituted orthoferrites.

In [19], a similar substitution in the $TbFe_{1-x}Mn_xO_3$ samples was discussed. Analyzing the changes in

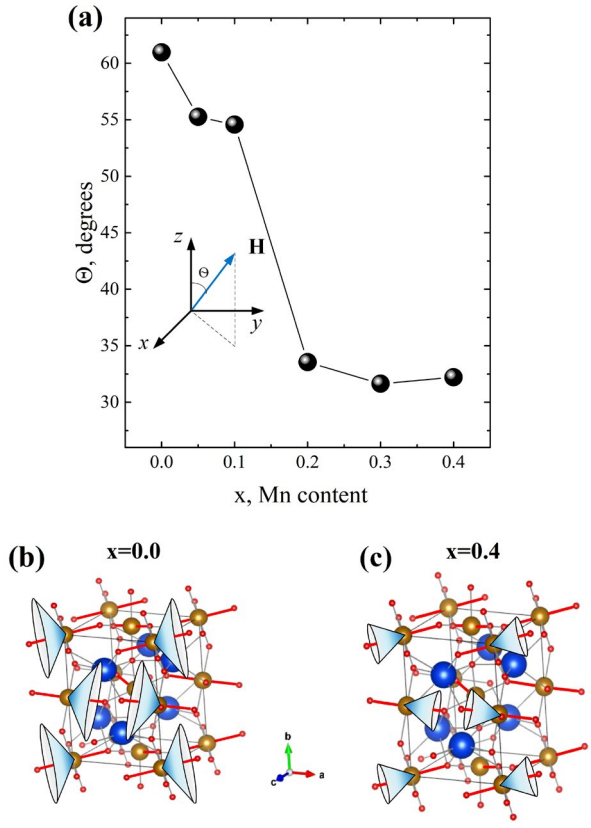

Fig. 12. (a) Dependence of the angle of mutual arrangement of the vectors of the main EFG component and hyperfine field on iron nuclei. (b) Schematic arrangement of the hyperfine field vectors (over the cone surface) and vector V_{zz} (bold line) at two extreme concentrations.

the indirect exchange in this system, the authors noted that the Mn substitution changes the magnetic moment orbital component, which is responsible for the magnetic structure formation. According to the Mössbauer data obtained, we can conclude that the change in the mutual orientation of the vectors V_{zz} and H_{hf} upon substitution results from the Jahn–Teller effect. This leads to the rotation of the magnetic moment both on Mn cations and on Fe cations and to a decrease in the weak ferromagnetic moment along the **b** crystal direction. This rotation of the magnetic moments in the subsystem of 3d cations in the $HoFe_{1-x}Mn_xO_3$ system can explain the growth of the temperature of the spin-reorientation transition.

5. CONCLUSION

In this study, a series of $HoFe_{1-x}Mn_xO_3$ single crystals over the entire substitute (Mn) concentration range was synthesized by the optical floating zone technique. It was found that, in the concentration range of $0.7 < x < 0.8$, the $HoFe_{1-x}Mn_xO_3$ compound undergoes a structural transition from the rhombic ($x < 0.7$) to hexagonal modification.

For the rhombic $HoFe_{1-x}Mn_xO_3$ modification, the magnetic measurements were performed, which showed that the spin-reorientation transition temperature T_{SR} increases significantly as the manganese content grows and, in the sample with $x = 0.4$, attains room temperature, which is important for application of the substituted orthoferrites.

It was found from the analysis of the magnetic measurement data that in all the substituted samples, the spin–reorientation transition is a first–order phase transition from the $A_xF_yG_z \rightarrow G_xC_yA_z$ phase with decreasing temperature, whereas in the initial $HoFeO_3$ sample, this is a second-order transition from the $A_xF_yG_z \rightarrow C_xG_yF_z$ phase.

An increase in the temperature of the spin–reorientation transition was attributed to a decrease in the value of the indirect Fe–O–Fe exchange under substitution of manganese for iron, which was established in the Mössbauer spectroscopy experiments.

FUNDING

This study was supported by the Russian Science Foundation, project no. 23–22–10026, https://rscf.ru/project/23-22-10026/ and the Krasnoyarsk Territorial Foundation for Support of Scientific and R&D Activities. The investigation of magnetic measurements and structural properties were performed using equipment from the Center for Collective Use, Krasnoyarsk Scientific Center, Siberian Branch of the Russian Academy of Sciences.

REFERENCES

1. R. White, *Review of recent work on the magnetic and spectroscopic properties of the rare-earth orthoferrites*,Journal of Applied Physics, **40**, 1061, (1969).

2. K. Belov, A. Zvezdin, and A. Kadomtseva, *New orientational transitions induced in orthoferrites by an external field*, J. Exp. Theor. Phys, **67**, (1974).

3. K. Belov, A. Zvezdin, A. Kadomtseva, and R. Levitin, *Orientational Transitions in Rare-Earth Magnets*, Nauka, Moscow, (1979).

4. K. Belov, A. Zvezdin, A. Mukhin, *Magnetic phase transitions in terbium orthoferrite*, Sov. Phys. JETP, **49**, 557, (1979).

5. A. Podlesnyak, S. Nikitin, and G. Ehlers, *Low-energy spin dynamics in rare-earth perovskite oxides*, Journal of Physics: Condensed Matter, **33**, 403001, (2021).

6. Y. Tokunaga, N. Furukawa, H. Sakai, Y. Taguchi, T.-h. Arima, and Y. Tokura, *Composite domain walls in a multiferroic perovskite ferrite*, Nature materials, **8**, 558, (2009).

7. A. Kimel, A. Kirilyuk, P. Usachev, R. Pisarev, A. Balbashov, and T. Rasing, *Ultrafast non-thermal control of magnetization by instantaneous photomagnetic pulses*, Nature, **435**, 655, (2005).

8. J. De Jong, A. Kimel, R. Pisarev, A. Kirilyuk, and T. Rasing, *Laser-induced ultrafast spin dynamics in* $ErFeO_3$, Physical Review B, **84**, 104421, (2011).

9. J. Jiang, Z. Jin, G. Song, X. Lin, G. Ma, and S. Cao, *Dynamical spin reorientation transition in* $NdFeO_3$ *single crystal observed with polarized terahertz time domain spectroscopy*, Applied Physics Letters, **103**, (2013).

10. S. Artyukhin, M. Mostovoy, N. P. Jensen, D. Le, K. Prokes, V. G. De Paula, H. N. Bordallo, A. Maljuk, S. Landsgesell, H. Ryll, et al., *Solitonic lattice and Yukawa forces in the rare-earth orthoferrite* $TbFeO_3$, Nature material, **11**, 694, (2012).

11. S. E. Nikitin, L. Wu, A. S. Sefat, K. A. Shaykhutdinov, Z. Lu, S. Meng, E. V. Pomjakushina, K. Conder, G. Ehlers, M. D. Lumsden, et al., *Decoupled spin dynamics in the rare-earth orthoferrite* $YbFeO_3$*: Evolution of magnetic excitations through the spin-reorientation transition*, Physical Review B, **98**, 064424, (2018).

12. K. Saito, A. Sato, A. Bhattacharjee, and M. Sorai, *High-precision detection of the heat-capacity anomaly due to spin reorientation in* $TmFeO_3$ *and* $HoFeO_3$, Solid state communications, **120**, 129, (2001).

13. A. Ovsianikov, O. Usmanov, I. Zobkalo, V. Hutanu, S. Barilo, N. Liubachko, K. Shaykhutdinov, K. Y. Terentjev, S. Semenov, T. Chatterji, et al., *Magnetic phase diagram of* $HoFeO_3$ *by neutron diffraction*, Journal of magnetism and magnetic materials, **557**, 169431, (2022).

14. J. Leake, G. Shirane, and J. Remeika, *The magnetic structure of thulium orthoferrite,* $TmFeO_3$, Solid State Communications, **6**, 15, (1968).

15. S. Skorobogatov, K. Shaykhutdinov, D. Balaev, M. Pavlovskii, A. Krasikov, and K. Y. Terentjev, *Spin dynamics and exchange interaction in orthoferrite* $TbFeO_3$ *with non-Kramers rare-earth ion*, Physical Review B, **106**, 184404, (2022).

16. S. Cao, H. Zhao, B. Kang, J. Zhang, and W. Ren, *Temperature induced spin switching in* $SmFeO_3$ *single crystal*, Scientific reports, **4**, 5960, (2014).

17. I. Dzyaloshinsky, *A thermodynamic theory of "weak" ferromagnetism of antiferromagnetics*, Journal of physics and chemistry of solids, **4**, 241, (1958).

18. T. Moriya, *Anisotropic superexchange interaction and weak ferromagnetism*, Physical review, **120**, 91, (1960).

19. Y. Fang, Y. Yang, X. Liu, J. Kang, L. Hao, X. Chen, L. Xie, G. Sun, V. Chandragiri, C.-W.Wang, et al., *Observation of re-entrant spin reorientation in* $TbFe_{1-x}Mn_xO_3$, Scientific reports, **6**, 33448, (2016).

20. J. Kang, Y. Yang, X. Qian, K. Xu, X. Cui, Y. Fang, V. Chandragiri, B. Kang, B. Chen, A. Stroppa, et al., *Spin-reorientation magnetic transitions in Mn-doped* $SmFeO_3$, IUCrJ, **4**, 598, (2017).

21. W. Fan, H. Chen, G. Zhao, X. Ma, R. Chakaravarthy, B. Kang, W. Lu, W. Ren, J. Zhang, and S. Cao, *Thermal control magnetic switching dominated by spin reorientation transition in* Mn*-doped* $PrFeO_3$ *single crystals*, Frontiers of Physics, **17**, 1, (2022).

22. L. Su, X.-Q. Zhang, Q.-Y. Dong, Y.-J. Ke, K.-Y. Hou, H.-t. Yang, and Z.-H. Cheng, *Spin reorientation and magnetocaloric effect of* $GdFe_{1-x}Mn_xO_3$ *(*$0 \leq x \leq 0.3$*) single crystals*, Physica B: Condensed Matter, **575**, 411687, (2019)

23. Z. Sun, H. Song, S. Zhu, X. Ma, W. Yang, C. Shi, B. Kang, R. Jia, J.-K. Bao, and S. Cao, *Pr-Doping Effect on Spin Switching in* $Nd_{0.8}Pr_{0.2}FeO_3$ *Single Crystal*, The Journal of Physical Chemistry C, **127**, 17592, (2023)

24. F.-K. Chiang, M.-W. Chu, F. Chou, H. Jeng, H. Sheu, F. Chen, and C. Chen, *Effect of Jahn-Teller distortion on magnetic ordering in* $Dy(FeMn)O_3$ *perovskites*, Physical Review B, **83**, 245105, (2011)

25. R. Vilarinho, D. Passos, E. Queir´os, P. Tavares, A. Almeida, M. Weber, M. Guennou, J. Kreisel, and J. A. Moreira, *Suppression of the cooperative Jahn-Teller distortion and its effect on the Raman octahedra-rotation modes of* $TbMn_{1-x}Fe_xO_3$, Physical Review B, **97**, 144110, (2018)

26. P. Mandal, V. S. Bhadram, Y. Sundarayya, C. Narayana, A. Sundaresan, and C. Rao, *Spin-reorientation, ferroelectricity, and magnetodielectric effect in* $YFe_{1-x}Mn_xO_3$ *(*$0.1 \leq x \leq 0.40$*)*, Physical review letters, **107**, 137202, (2011)

27. G. Song, J. Su, S. Fang, J. Tong, X. Xu, H. Yang, and N. Zhang, *Modified crystal structure, dielectric and magnetic properties of Cr doped* $SmFeO_3$ *ceramic*, Physica B: Condensed Matter, **589**, 412185, (2020)

28. Z. Habib, M. Ikram, K. Sultan, Abida, S. A. Mir, K. Majid, and K. Asokan, *Electronic excitation-induced structural, optical, and magnetic properties of* Ni-*doped* $HoFeO_3$ *thin films*, Applied Physics A, **123**, 1, (2017)

29. A. Somvanshi, S. Husain, S. Manzoor, N. Zarrin, N. Ahmad, B. Want, and W. Khan, *Tuning of magnetic properties and multiferroic nature: case study of cobalt-doped* $NdFeO_3$, Applied Physics A, **127**, 1, (2021)

30. P. Prakash, V. Sathe, C. Prajapat, A. Nigam, P. Krishna, and A. Das, *Spin phonon coupling in* Mn *doped* $HoFeO_3$ *compounds exhibiting spin reorientation behaviour*, Journal of Physics: Condensed Matter, **32**, 095801, (2019)

31. S. Yuan, Y. Yang, Y. Cao, A. Wu, B. Lu, S. Cao, and J. Zhang, *Tailoring complex magnetic phase transition in* $HoFeO_3$, Solid state communications, **188**, 19, (2014)

32. L. Holmes, L. Van Uitert, and R. Hecker, *Effect of Co on magnetic properties of* $ErFeO_3$*,* $HoFeO_3$*, and* $DyFeO_3$, Journal of Applied Physics, **42**, 657, (1971)

33. G. P. Vorob'ev, A. M. Kadomtseva, I. B. Krynetkii, and A. A. Mukhin, *Unusual nature of spin reorientation in* $HoFeO_3$, Zh. Eksp. Teor. Fiz, **95**, 1049, (1989)

34. A. M. Balbashov, G. V. Kozlov, S. P. Lebedev, A. A. Mukhin, A. Y. Pronin, and A. S. Prokhorov, *Anomalies of high-frequency magnetic properties and new orientational transitions in* $HoFeO_3$, Zh. Eksp. Teor. Fiz, **95.3**, 1092, (1989)

35. G. Durbin, C. Johnson, L. Prelorendjo, and M. Thomas, *Spin reorientation in rare earth orthoferrites*, Le Journal de Physique Colloques, **37**, C6, (1976)

36. Y. Sundarayya, P. Mandal, A. Sundaresan, and C. Rao, *Mössbauer spectroscopic study of spin reorientation in Mn-substituted yttrium orthoferrite*, Journal of Physics: Condensed Matter, **23**, 436001, (2011)

37. W. Kim, B. Y. Kum, and C. S. Kim, *Spin-Reorientation and Mössbauer Study of Orthoferrite* $TbFe_{0.75}Mn_{0.25}O_3$, Journal of superconductivity and novel magnetism, **24**, 867, (2011)

38. D. Ryan, Q. Stoyel, L. Veryha, K. Xu, W. Ren, S. Cao, *A Single-Crystal Mössbauer Study of Spin Reorientations in the Multi-Ferroic* $HoFeO_3$, IEEE Transactions on Magnetics, **53**, 1, (2017)

39. P. Gütlich, E. Bill, and A. X. Trautwein, *Mössbauer spectroscopy and transition metal chemistry: fundamentals and applications*, Springer Science & Business Media, (2010)

40. N. Lee, Y. Choi, M. Ramazanoglu, I. W Ratcliff, V. Kiryukhin, and S.-W. Cheong, *Mechanism of exchange striction of ferroelectricity in multiferroic orthorhombic* $HoMnO_3$ *single crystals*, Physical Review B, **84**, 020101, (2011)

41. A. Dubrovskiy, N. Pavlovskiy, S. Semenov, K. Y. Terentjev, and K. Shaykhutdinov, *The magnetostriction of the* $HoMnO_3$ *hexagonal single crystals*, Journal of Magnetism and Magnetic Materials, **440**, 44, (2017)

42. V. J. Angadi, K. Manjunatha, S. Kubrin, A. Kozakov, A. Kochur, A. Nikolskii, I. Petrov, S. Shevtsova, and N. Ayachit, *Crystal structure, valence state of ions and magnetic properties of* $HoFeO_3$ *and* $HoFe_{0.8}Sc_{0.2}O_3$ *nanoparticles from* X*-ray diffraction,* X*-ray photoelectron, and* M*össbauer spectroscopy data*, Journal of Alloys and Compounds, **842**, 155805, (2020)

43. P. Pina, R. Buentello, H. Arriola, and E. Nava, *Mössbauer spectroscopy of lanthanum and holmium ferrites*, Hyperfine Interactions, **185**, 173, (2008)

44. R. Sternheimer, *On nuclear quadrupole moments*, Physical Review, **80**, 102, (1950)

45. R. Sternheimer, *On nuclear quadrupole moments*, Physical Review, **84**, 244, (1951)

46. L. S. V. R. Marathe, and A. Trautwein, *Sternheimer shielding using various approximations*, Physical Review A, **19**, 1852, (1979)

47. H. Brinks, J. Rodríguez-Carvajal, H. Fjellvåg, A. Kjekshus, and B. Hauback, *Crystal and magnetic structure of orthorhombic* $HoMnO_3$, Physical Review B, **63**, 094411, (2001)

48. I. Lyubutin, P. Naumov, B. Mill, K. Frolov, and E. Demikhov, *Structural and magnetic properties of the iron-containing langasite family* $A_3MFe_3X_2O_{14}$ *(*$A = Ba, Sr; M = Sb, Nb, Ta; X = Si, Ge$*) observed by* M*össbauer spectroscopy*, Physical Review B, **84**, 214425, (2011)

49. E. O. Wollan, and W. C. Koehler, *Neutron Diffraction Study of the Magnetic Properties of the Series of Perovskite-Type Compounds* $[(1–x)La, xCa]MnO_3$, Physical Review, **100.2**, 545, (1955)

50. J. Hemberger, M. Brando, R. Wehn, V. Y. Ivanov, A. A. Mukhin, A. M. Balbashov, and A. Loidl, *Magnetic properties and specific heat of* $RMnO_3(R = Pr, Nd)$, Physical Review B, **69.6**, 064418, (2004)